Scuffing initiation caused by local starvation in a piston ring cylinder liner contact

Simona Dahdah, Nans Biboulet, Antonius Adrianus Lubrecht, Pierre Charles

Scuffing initiation caused by local starvation in a piston ring cylinder liner contact

*Simona Dahdah[1,2], Nans Biboulet[1], Antonius Lubrecht[1], Pierre Charles[2]
[1] Univ Lyon, INSA-Lyon, CNRS UMR5259, LaMCoS, F-69621, France.
[2] Stellantis, route de Gisy, 78140 Vélizy Villacoublay, France.

*Corresponding author:
simona.dahdah@insa-lyon.fr
32 Rue Jules Vallès, 69100 Villeurbanne-France

Abstract

Scuffing is a localized damage process caused by a sudden failure of the lubricating film in a sliding contact. It is associated with an important increase in temperature, friction and vibration. For the piston-ring cylinder-liner (PRCL) contact, it can lead to a complete engine failure. It is shown in this paper, that the temperature gradient generated in the contact induces the thermal Marangoni effect. The latter might then lead to a localized lack of lubricant that can initiate scuffing. On the contrary, the ring displacement along the liner redistributes the oil on the surface. This redistribution helps to avoid starvation hence reducing scuffing initiation risk. Based on the competition occurring between these two effects, a computational model was developed that predicts scuffing appearance in internal combustion engines. The originality of this paper lies in presenting the complementary contribution of the Marangoni phenomenon to the scuffing initiation in the PRCL contact.

Keywords: Scuffing, PRCL contact, Lubrication, Marangoni effect

1 Introduction

The automotive industry is facing a customer demand for powerful vehicles and the environmental protection requirements for lower pollutant emissions. One possible way to reduce emissions is to reduce engine power losses. The frictional loss occurring in the Piston-Ring/Cylinder-Liner (PRCL) contact is estimated to be about half of the total engine friction loss [1]. In addition, this contact is exposed to several failure modes that might affect the overall engine performance and lifetime. For these reasons, the understanding of the phenomena acting in this contact as well as optimizing its lubrication mechanism have attracted the attention of researchers.

Wear is a common failure that can take place in the contact, it is a slowly progressing mechanism [2]. Scuffing is an uncommon failure process and its occurrence in the internal combustion engine is rare, but once it initiates, the damage is catastrophic. Hence, the importance of studying and predicting its initiation.

Scuffing is the least understood tribological failure because of the large number of variables involved in its initiation and the diversity of machine operating conditions. It occurs primarily in a lubricated contact with sliding bodies [3]. It is commonly accompanied by a sudden increase in friction, temperature and vibration [4].

Numerous definitions are proposed to describe this failure such as: “gross damage characterized by formation of local welds between sliding surfaces” [5], “surface roughening by plastic flow whether or not there is material loss or transfer” [2] and “localized damage caused by solid-phase welding between sliding surfaces” [6]. An additional description of scuffing is provided by the ASTM committee: “a form of wear occurring in inadequately lubricated tribo-systems that is characterized by macroscopically-observable changes in surface texture” [7].

Dyson [5] considered that the failure of the lubricating film is the main reason for scuffing initiation. Shuster et al. [8] and Obert et al. [9] showed in their experimental studies that the oil quantity and the temperature are vital parameters.

Another approach of scuffing is studied by Shen et al. [10], they concluded that the lubricant desorption leads to an increase in friction and then accelerates scuffing initiation. The rate of lubricant desorption increases with the temperature as shown by Li et al. [11] when the lubricant decomposition under heating test is studied.

Qu et al. and Van et al. [12, 13] showed that scuffing initiates in the vicinity of the top dead center where the lubrication conditions are the worst. Barunovis et al. [14] reported wear maps and scuffing limits for a pin on disc model test as a function of the contact load and the sliding speed. From these maps, one can conclude that scuffing is reached sooner when the speed increases. Based on that, exists a probability that scuffing may occur at mid-stroke where the velocity is high.

Another approach for scuffing prediction is based on the shear stress. Scuffing initiates when the shear stress exceeds the critical one, this is observed when plastic deformation occurs [15]. The shear stress was identified to depend on the lubricant additives. [16].

The time to scuff depends on the surface material and its wear resistance as shown by Wan et al [17]. Surface coatings such as Carbon-based, diamond-like are used for components operating in a solid-to-solid contact [18–20]. They increase the surface scuffing resistance and delay the scuffing initiation [4, 21–23]. However, when oil starvation occurs, friction and wear increase progressively which can lead to a total removal of the coating. Subsequently, the metal-to-metal contact increases the

probability of scuffing initiation.
Moreover, the insufficient oil supply to the PRCL contact might cause it to operate under mixed lubrication conditions [24–28] therefore increasing the friction. This local increase in friction generates a local heat flux which in turn generates a temperature gradient. The latter engenders a surface tension gradient that causes an oil displacement, hence, a possible oil film rupture exists as mentioned by Fantom et al. [29] and Monti et al. [30]. This effect is known as the thermal Marangoni effect, which relates the fluid motion to the surface tension gradient generated by the temperature gradient, see Gugliotti et al. [31].
The oil redistribution effect caused by the ring displacement along the liner is a counteracting phenomenon, see Organisciak et al. [32]. The oil redistribution is beneficial for the PRCL contact lubrication performance since it helps to avoid the local starvation thus the scuffing initiation [33].
These two opposing mechanisms affect the lubricant distribution in the PRCL contact: the thermal Marangoni process tends to create a localized starved zone and the ring displacement spreads oil along the contact and helps to avoid starvation. The current paper highlights the competition occurring between the Marangoni and the ring displacement effects which is the basis of a computational model for scuffing initiation prediction in the piston ring cylinder liner contact of engines.

2 Model

The temperature of the liner and the ring surfaces is initially considered constant and equal to T_0. However, when considering the occurrence of a temporarily local lack of lubricant due to a non-uniform oil distribution in the contact, the coefficient of friction increases (see figure 1). Then, an additional heat flux is locally generated. The additional heat flux generated ($q_{heated-zone}$) is given in the equation below:

$$q_{heated-zone} = \zeta \mu p_{contact} u_m \tag{1}$$

where μ is the coefficient of friction, $p_{contact}$ is the contact pressure (equation 2), u_m is the mean velocity (equation 3) of the ring and ζ is the ratio of the heat exchange occurring between the liner and the ring. Its value ranges from 0 to 1. 0 meaning that there is no heat transferred to the surface whilst 1 means that the heat is totally transferred to the surface.
The coefficient of friction is defined via the Stribeck curve (figure 1) as a function of the ratio of the oil film thickness (h_0) divided by the surface roughness (σ). From the curve, it can be concluded that the lower the film thickness, the higher the coefficient

of friction. Note that σ is considered constant in the model and that the values given in the curve are generic ones.
The mean contact pressure ($p_{contact}$) applied by the ring itself is calculated from the ring tension (F_{ring}) via equation 2.

$$p_{contact} = \frac{2F_{ring}}{\varphi\, t_{axial}} \tag{2}$$

where φ is the nominal ring diameter and t_{axial} is the ring axial thickness. As the piston ring velocity varies along the stroke (low at the top and bottom dead centers and high at mid-stroke), the mean ring velocity (u_m) along the stroke is used in the model. It depends on the engine frequency in *rpm* (N) and the stroke length (C) as shown in equation 3. It increases with the engine speed. As the engine speed and the stroke distance are both considered constants in the model, the piston velocity is also constant.

$$u_m = \frac{NC}{30} \tag{3}$$

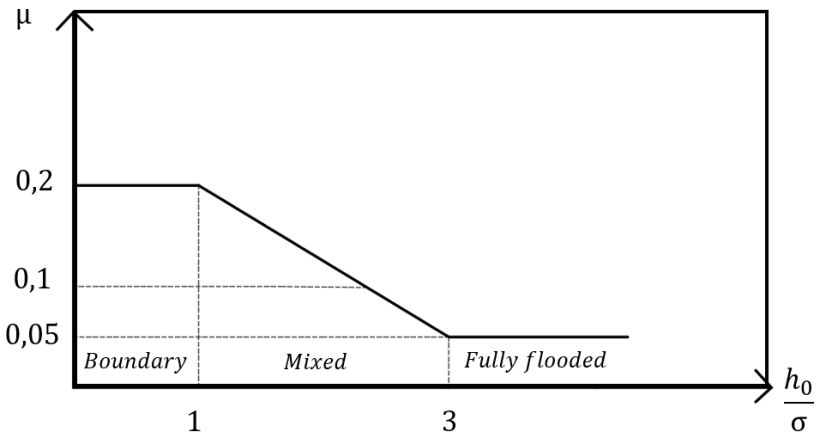

Figure 1: Stribeck curve: coefficient of friction as a function of the oil film thickness divided by the surface roughness

2.1 Thermal model

2.1.1 Thermal assumptions

Several thermal assumptions have been used to simplify the model:

the material is considered to be isotropic; the conductivity is the same in all directions,

there is no heat stored in the lubricant,

the heat exchange occurring between the liner and the ring surfaces with their surroundings is not studied in the current model,

Neumann boundary conditions are used to simulate the heat flux generated in the starved/heated zone (q imposed), whilst Dirichlet boundary conditions (T_0 imposed) are used elsewhere, where T_0 is the nominal liner temperature at which minimum friction occurs, its upper bound is approximately 140 C [34]. This is the simplest boundary condition to be considered to simplify the model.

The ring is moving along the liner in the x-direction as shown in figure 2. Thus, a transient 3D model is required to calculate the liner temperature distribution.

Figure 2: Liner surface with a moving heat flux

To simplify the model, the generated heat flux is averaged over the time of a ring passage along the liner. The average time of a ring passage is $\Delta t_{passage} = 1/(2f)$, where f is the frequency in Hz. The required time for the heat flux to change position is $\Delta t = t_{axial}/u_m$. The mean heat flux is then obtained as shown below:

$$q_{mean} = \zeta \mu p_{contact} u_m \frac{\Delta t}{\Delta t_{passage}} = \zeta 2 \mu p_{contact} t_{axial} f \quad (4)$$

The liner surface exposed to the mean heat flux (q_{mean}) is presented in figure 3. As the heat flux and the temperature-increase are constant along the liner, and the surface is considered infinitely long in the x-direction, the transient 3D model is simplified to a stationary 2D model. Note that in this example $q_{mean} = \zeta 2 \mu p_{contact} t_{axial} f = 1 * 2 * 0.1 * 10^6 * 1.5e^{-}3 * 60 = 18 * 10^3 W/m^2$.

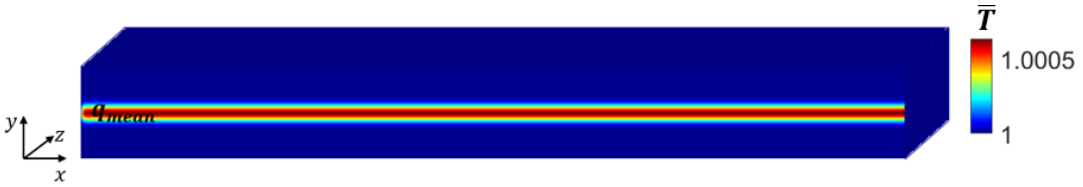

Figure 3: Liner surface with mean heat flux

Figure 4 shows the 2D liner thermal model in the (y–z) plane used for the temperature distribution calculation where s refers to the width of the starved/heated zone. The domain size (s_d) is wide enough to guarantee that the Dirichlet boundary conditions do not influence the temperature increase calculation.

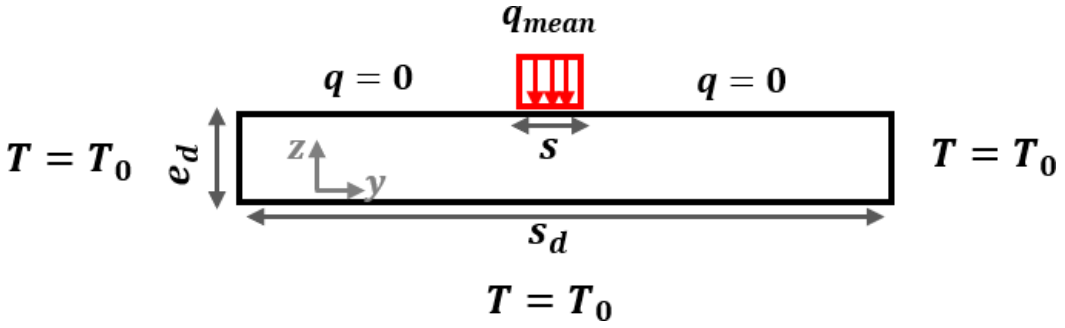

Figure 4: 2D liner thermal model

2.1.2 Equations

The stationary 2D Fourier heat equation without considering an internal heat source is:

$$\frac{\partial}{\partial y}\left(\alpha_y \frac{\partial T}{\partial y}\right) + \frac{\partial}{\partial z}\left(\alpha_z \frac{\partial T}{\partial z}\right) = 0 \quad (5)$$

where α_y, α_z are the conductivity in respectively y and z directions. As the material is isotropic hence, $\alpha_y=\alpha_z=\alpha$.

The dimensionless 2D Fourier heat equation is:

$$\frac{\partial^2 \bar{T}}{\partial Y^2} + \frac{\partial^2 \bar{T}}{\partial Z^2} = 0 \quad (6)$$

The thermal equation is solved numerically to obtain the temperature variation required for the study. More details about the equation discretization and resolution are given in appendix 5.

Equations 7 and 8 show respectively the lubricant surface tension and viscosity as a function of the temperature.

$$\gamma = \gamma_0 \left(1 - \frac{T}{T_c}\right)^n \quad (7)$$

$$\log(\log(\eta + 0.7)) = a \log(T) + b \quad (8)$$

The dimensionless surface tension and viscosity are respectively $\bar{\gamma} = \gamma/\gamma_0$ and $\bar{\eta} = \eta/\eta_0$.

Where γ_0 and η_0 are the surface tension and the viscosity of the lubricant at the reference temperature T_0. T_c is the critical temperature of the lubricant and a and b are constants depending on the lubricant. Note that the lubricant used in the model is a typical, commercial car engine oil.

2.2 Marangoni effect

The lubricant displacement due to the Marangoni effect is shown in figure 5. Note that the lubricant curvature is exaggerated in the figure and that the forces due to that curvature are negligible.

The oil flows from the high temperature zone where the surface tension is low (low γ zone) to the low temperature zone where the surface tension is high (high γ zone) and it is submitted to the following stresses:

the Marangoni stress:

$$\tau_{Marangoni} = \frac{\partial \gamma}{\partial y} \quad (9)$$

the viscous stress:

$$\tau_{viscous} = \eta \frac{v}{h} \tag{10}$$

The variation of the oil film thickness as a result of the Marangoni effect is given by equation 13. It is the result of the combination of two equations:

the equilibrium of the Marangoni and the viscous stresses ($\tau_{Marangoni}=\tau_{viscous}$), from where the equation of the oil velocity (v) is obtained:

$$v = \frac{h}{\eta}\frac{\partial \gamma}{\partial y} \tag{11}$$

the equilibrium of the variation of the oil film over time ($\partial h/\partial t$) and the Couette flux ($\partial \varphi_c/\partial y$) along the y direction ($\partial h/\partial t=\partial \varphi_c/\partial y$),

where

$$\varphi_c = \frac{vh}{2} \tag{12}$$

The velocity term in equation 12 is replaced by equation 11 and the second equilibrium is solved to obtain the Marangoni equation:

$$\frac{\partial h}{\partial t} = -\frac{\partial}{\partial y}\left(\frac{h^2}{2\eta}\frac{\partial \gamma}{\partial y}\right) \tag{13}$$

The dimensionless Marangoni equation is:

$$\frac{\partial H}{\partial \bar{t}} = -\frac{\partial}{\partial Y}\left(\frac{H^2}{2\bar{\eta}}\frac{\partial \bar{\gamma}}{\partial Y}\right) \tag{14}$$

Appendix 5 details the Marangoni equation discretization and resolution.

2.3 Oil redistribution effect

2.3.1 Hydrodynamic assumptions

The hydrodynamic assumptions considered to obtain a simple and stationary model are:

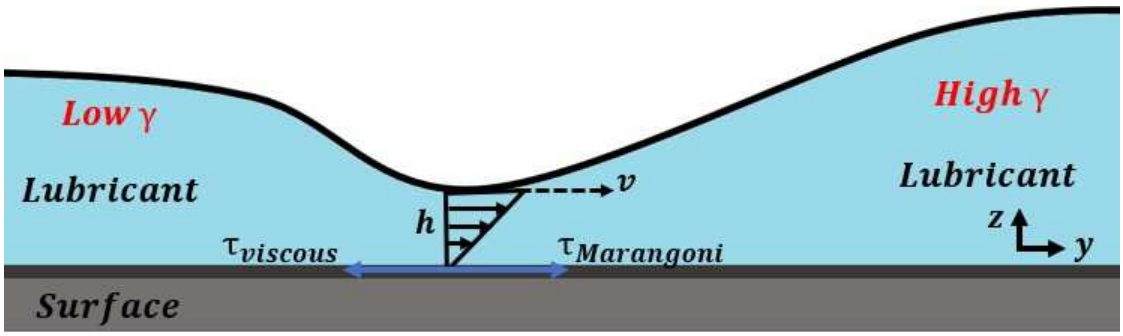

Figure 5: Thermal Marangoni model

the PRCL contact is considered as a hydrodynamic lubricated contact, meaning that the contacting surfaces are rigid,

the ring velocity is constant along the *x*-direction and equal to the mean speed,

the surface roughness is considered constant and surface texturing is not taken into consideration to decrease the number of the parameters,

the lubricant viscosity is considered constant in the contact and independent of the local temperature and pressure,

the squeeze effect is negligible, which describes the variation of the film thickness as a function of time.

2.3.2 Equations

The iso-viscous, constant density and steady-state Reynolds equation describing the flow of a thin film lubricant between two surfaces for a fully flooded lubrication regime is presented below:

$$\frac{1}{12\eta}\frac{\partial}{\partial x}\left(h^3\frac{\partial p}{\partial x}\right)+\frac{1}{12\eta}\frac{\partial}{\partial y}\left(h^3\frac{\partial p}{\partial y}\right)=u_m\frac{\partial h}{\partial x} \tag{15}$$

The steady-state assumption is valid as the liner surface is considered to be smooth and the oil film variation is negligible. In the starved lubrication regime, a limited amount of oil is available in the contact and the pressurized zone is narrower than in the fully flooded regime. To analyze the fluid film under starved conditions, a parameter ϑ is introduced which is the void fraction (1-ratio between the oil film

thickness (h_{oil}) and the geometry gap between the surfaces (h)). Its value ranges from 0 to 1 ($0 \leq \vartheta \leq 1$). The Reynolds equation is then modified to take into consideration ϑ and describes the starved lubrication regime.

$$\frac{1}{12\eta}\frac{\partial}{\partial x}\left(h^3\frac{\partial p}{\partial x}\right)+\frac{1}{12\eta}\frac{\partial}{\partial y}\left(h^3\frac{\partial p}{\partial y}\right)=u_m\frac{\partial\left((1-\vartheta)\,h\right)}{\partial x} \tag{16}$$

The dimensionless equation is:

$$\frac{\partial}{\partial X}\left(H^3\frac{\partial P}{\partial X}\right)+\frac{\partial}{\partial Y}\left(H^3\frac{\partial P}{\partial Y}\right)-\frac{\partial\left((1-\vartheta)\,H\right)}{\partial X}=0 \tag{17}$$

In order to study the ring displacement impact on the oil distribution, a circumferentially non-uniform oil geometry is imposed at the inlet of the contact as shown in figure 6. The oil distribution is obtained by equation 18. A mass-conserving solver is used for the solution of the Reynolds equation, see Biboulet and Lubrecht [35]. The calculation output are the pressure and the circumferential oil distribution after the passage of the ring. The redistribution is studied and quantified by comparing the oil geometry imposed and the one obtained after the ring passage.

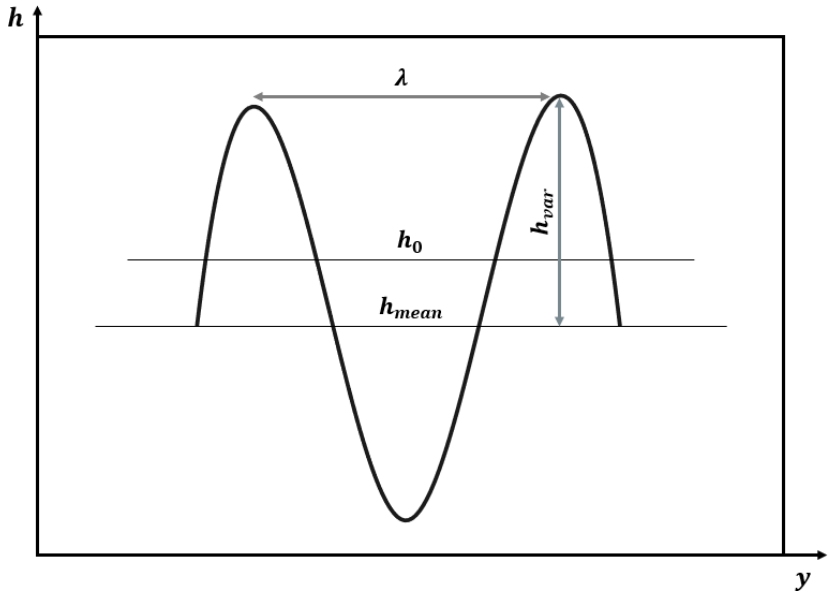

Figure 6: Oil distribution geometry

$$h_{oil}(y) = h_{mean} - h_{var}\cos(\frac{2\pi y}{\lambda}) \quad (18)$$

where:

h_{mean} is the average oil film thickness,

h_{var} is the oil variation with respect to h_{mean}, it defines the maximum and the minimum thickness of the oil film at the inlet of the contact,

λ is the wavelength.

2.4 Lubricant distribution model

Figure 7 presents a schematic of the lubricant distribution in the contact. Assuming that under certain operating conditions, a local lack of lubricant might temporarily occur due to an oil displacement and a non-uniform oil distribution in the contact. As a result, the coefficient of friction increases which in turn leads to a temperature increase of the liner surface (ΔT) compared to the initial surface temperature (T_0). The surface tension and viscosity gradients depending on the temperature are obtained (equations 7 and 8). The oil film thickness (h_0) is then calculated using equation 19 [36].

$$h_0 = 2.45\frac{\eta u_m R_x}{w_1} \quad (19)$$

where R_x is the radius of curvature and w_1 is the load per unit length.

A Marangoni calculation is then carried out to predict the oil variation (h_{var}) caused by the surface tension gradient compared to the mean film thickness (h_{mean}) which is considered to be equal to the oil film thickness ($h_{mean} = h_0$).

The last part quantifies the following surfaces:

the surface displaced due to the Marangoni effect ($S_{Marangoni}$) as a function of the temperature increase (ΔT), the oil film thickness (h_0), the lubricant surface tension and viscosity gradients. In fact, the volume flow rate of the displaced oil is presented as a moving surface in order to compare it to the one moved due to the ring passage,

the surface moved due to the ring passage ($S_{redistributed}$) as a function of the oil film thickness and the oil geometry distribution parameters (h_{mean}, h_{var} and λ).

If $S_{Marangoni}$ is larger than $S_{redistributed}$ ($S_{Marangoni}$>$S_{redistributed}$), which means that the lubricant starvation caused by the Marangoni effect is more pronounced than the lubricant redistribution caused by the ring passage, scuffing might initiate. One has to note that these two opposing effects are repetitive and occur at every engine cycle, meaning that the imbalance can be accumulated then leading to a localized lack of lubricant after a sufficient number of cycles. Else, when starvation is balanced by the oil redistribution, the local lack of lubricant is avoided and no risk of scuffing exists.

The purpose of this model is to study the contact performance when it is exposed to local heating yet the lubricant is re-supplied. The question to explore is that despite the local heating, will the contact perform normally when it is re-lubricated?

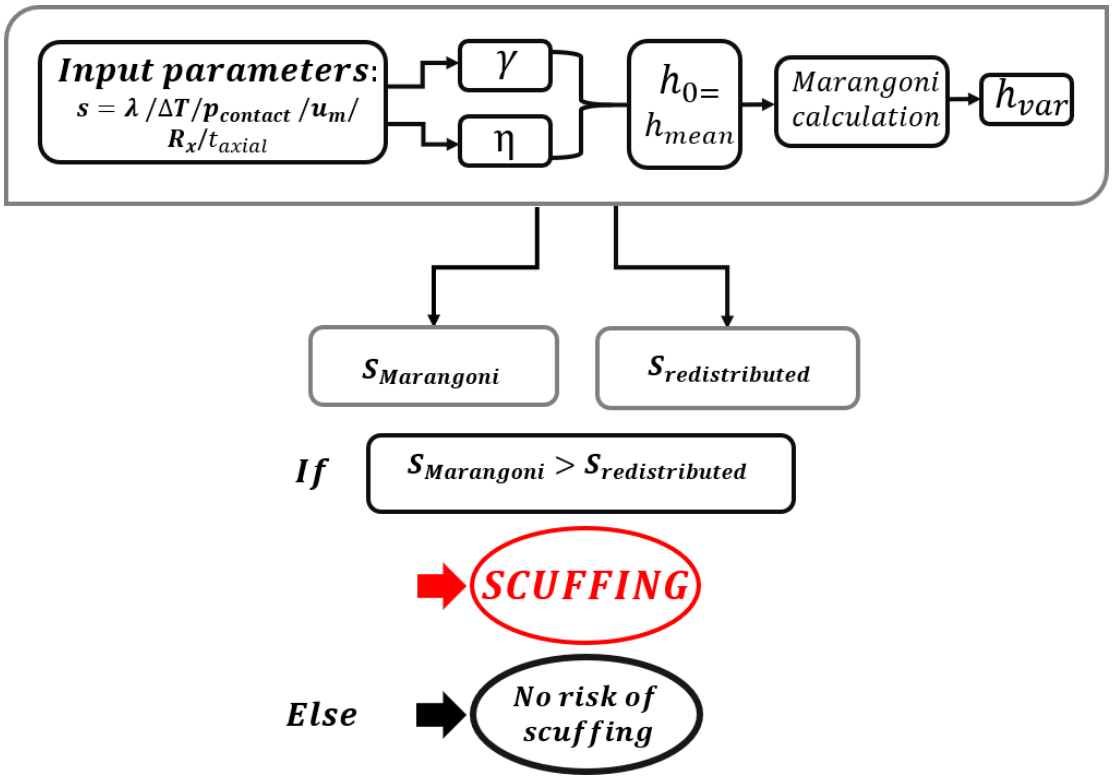

Figure 7: Lubricant distribution model

3 Results

The values of the input parameters used in this section are given in tables 3 and 4. Figure 3 shows the temperature distribution when the average heat flux is q_{mean} = $18 * 10^3 W/m^2$. The temperature increase due to q_{mean} is $\Delta T = 0.1815K$ (when considering that $T_0 = 363K$, $\Delta T = 1.0005T_0 - T_0$). This temperature increase is negligible and insufficient to generate the Marangoni effect and to consider the probability of failure risk. Thus, in the following study, the temperature increase compared to the nominal temperature is imposed as an input parameter, instead of the heat flux. Then, the heat flux needed to be injected to cause the chosen temperature increase is known. Therefore, the temperature distribution required for the Marangoni calculation is obtained. Note that the relation between the heat flux and the temperature increase is linear ($q = c\Delta T$), where c is a constant.

3.1 Lubricant displacement

3.1.1 Temperature gradient

Assuming in this example that the width of the starved/heated zone occurring on the liner surface is $s = 4.4mm$, the nominal surface temperature is $T_0 = 363K$ and the temperature increase is $\Delta T = 20K$. Then, the heat flux (q) to be injected is computed and it is imposed as a Neumann condition over s. The 2D Fourrier equation (equation 6) is solved to calculate the temperature distribution. The latter is shown in figure 8. Note that the temperature increase is $\Delta T = (1.055 - 1)(T_0)$. As shown in the figure, the highest temperature is located in the middle of the contact and the temperature gradient extends from $Y = -1$ to $Y = 1$, this is the starved/heated zone.

As a consequence of the temperature gradient, a lubricant surface tension gradient is generated as shown in figure 9. The increase in temperature leads to a decrease in the lubricant surface tension (equation 7), so the surface tension has its lowest value in the heated zone. In addition, the temperature gradient leads to a lubricant viscosity gradient as shown in figure 10, and the increase in the temperature decreases the lubricant viscosity (equation 8).

3.1.2 Influence of the temperature gradient

Starting with the hypothesis that an increase in the temperature occurs in the contact due to a localized lack of lubricant, the temperature, surface tension and viscosity distributions are defined and a Marangoni calculation is carried out (equation 13).

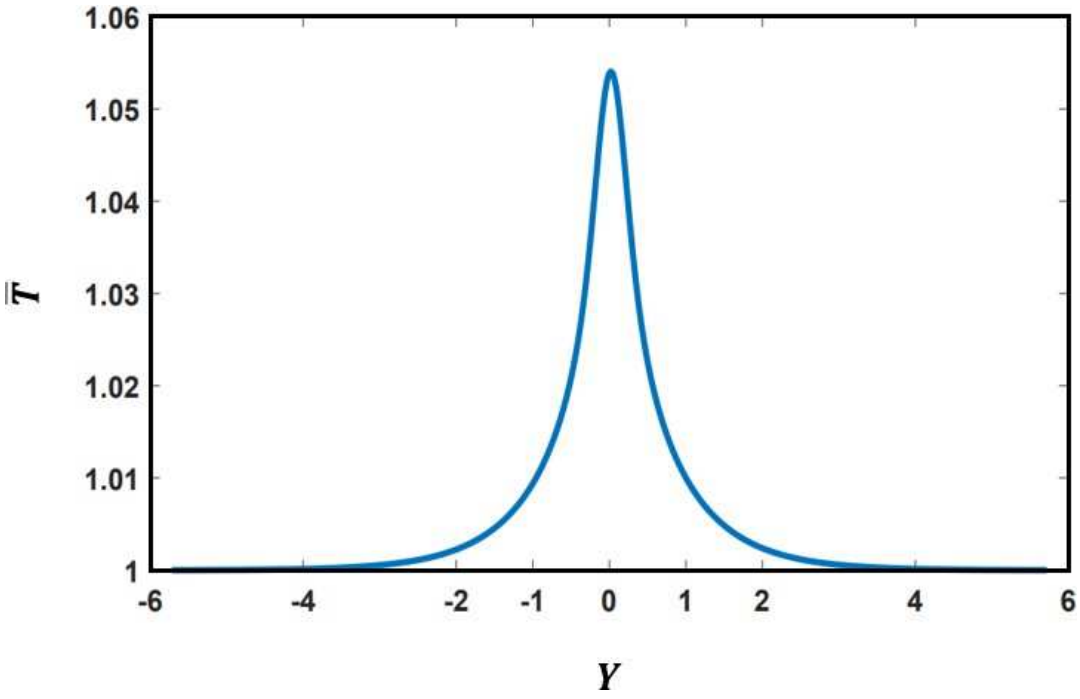

Figure 8: Dimensionless temperature distribution generated on the liner surface

Figure 11 shows the lubricant film thickness variation in the circumferential direction caused by the Marangoni effect for different temperature increases. One can conclude that the maximum lubricant thickness variation is located in the heated zone. This is caused by the decrease in the lubricant surface tension. In fact, the lubricant tends to flow from the warmer zone (where the surface tension is at its lowest value) to the colder zone (where the surface tension is at its highest value). Note that the displacement caused by the Marangoni effect is continuous and lasts for a period of a passage ($t_{passage} = C/u_m$). Furthermore, the film thickness decrease is proportional to the temperature increase, and more precisely to the temperature gradient since the source width is kept constant in these examples ($s = 4.4mm$). The surface difference (ΔS) between the initial oil distribution for $\Delta T = 0$ and the one corresponding to $\Delta T \neq 0$ represents the oil flux displaced as a result of the Marangoni effect and it is called $S_{Marangoni}$. To quantify the oil flow, the surface difference is calculated as a function of the model parameters.

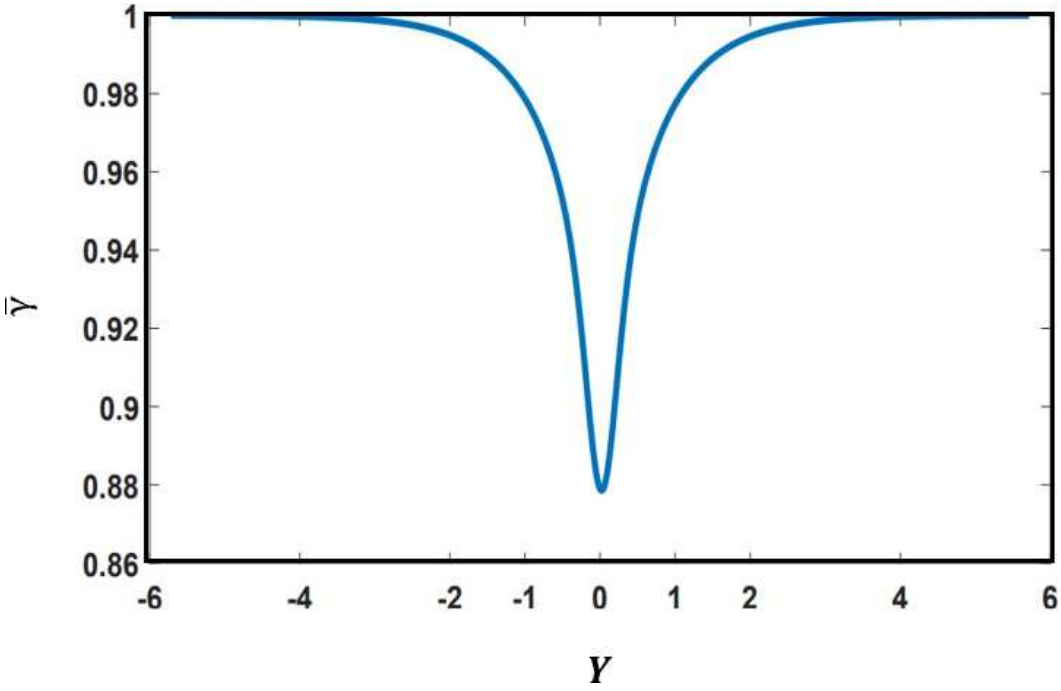

Figure 9: Dimensionless lubricant surface tension distribution

3.1.3 Analytic oil flow

In order to quantify the displacement caused by the Marangoni effect, the differential equation 13 is analytically developed so the surface moved ($S_{Marangoni}$) can be obtained by equation 20.

$$S_{Marangoni} = s\frac{h_0^2}{2}\left[\frac{\partial\,(1/\eta)}{\partial y}\frac{\partial \gamma}{\partial y} + \frac{1}{\eta}\frac{\partial^2 \gamma}{\partial y^2}\right] t_{passage} \tag{20}$$

The development is detailed below:

$$S_{Marangoni} = \Delta S = s\Delta h \tag{21}$$

The expression of Δh is obtained from equation 20:

$$\Delta h = \frac{h^2}{2}\cdot\left[\frac{\partial}{\partial y}\frac{1}{\eta}\frac{\partial \gamma}{\partial y} + \frac{1}{\eta}\frac{\partial^2 \gamma}{\partial y^2}\right] t_{passage} \tag{22}$$

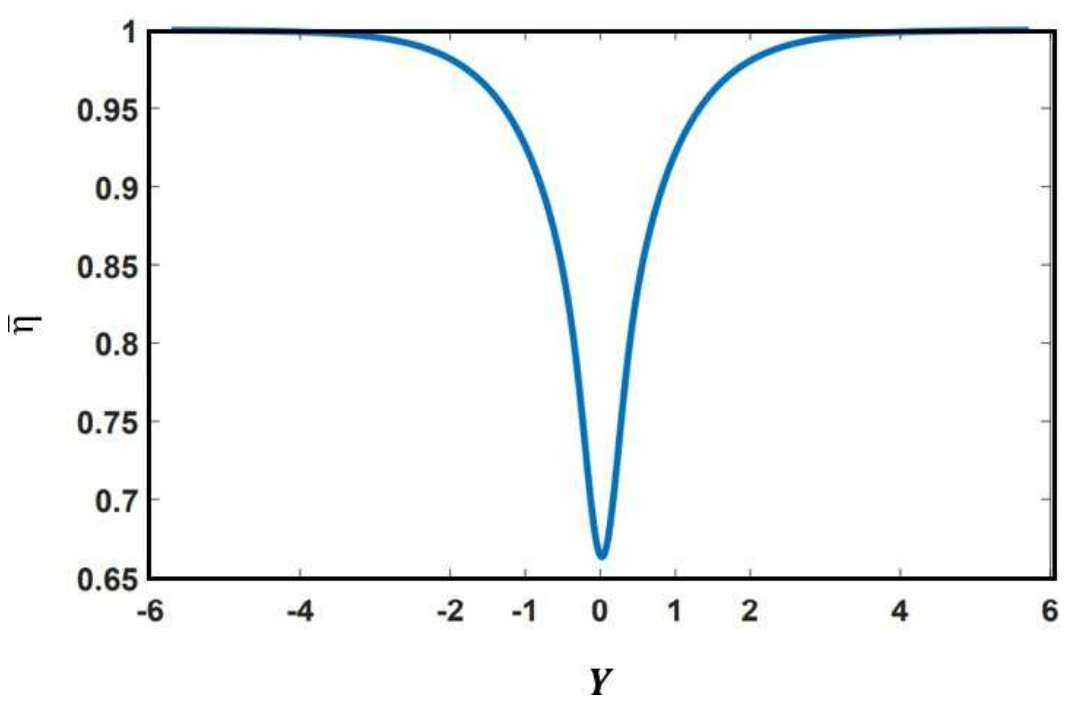

Figure 10: Dimensionless lubricant viscosity distribution

Δh in equation 21 is replaced by equation 22 then equation 20 is obtained.

As the equation shows, the displacement depends on the oil film thickness, the local temperature, the temperature increase, the surface tension and viscosity gradients and the time of passage.

3.1.4 Influence of the engine speed

The influence of the engine speed on the surface moved due to the Marangoni effect is studied. The temperature increase is $20K$, the width of the heated zone is $s = 4.4mm$ and the oil supply regime is moderately starved. Note that if h_{ff} is the oil film thickness in a fully flooded supply regime, the oil film thickness in a moderately starved regime is $h_{ff}/3$.

The increase in engine speed leads to:

an increase in the mean velocity (u_m), hence an increase in the oil film thickness (h_0) (equations 3 and 19),

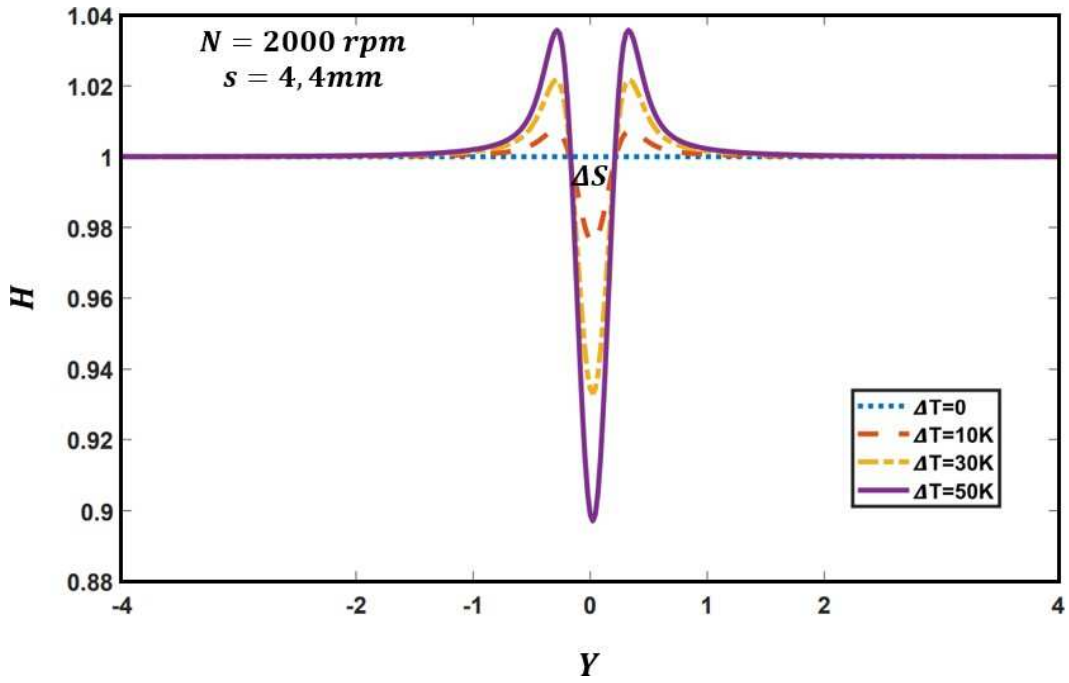

Figure 11: Dimensionless film thickness variation along the circumferential direction for different temperature increase values

a decrease in the passage time ($t_{passage}$).

As shown in equation 20, the Marangoni effect depends on the oil quantity and on the time of passage. For an imposed temperature increase, it is more pronounced when the oil quantity and/or the passage time increases.
Figure 12 shows that $S_{Marangoni}$ increases with the engine speed. This result indicates that the sensibility of the oil quantity on the surface moved is more important than that of the time passage.

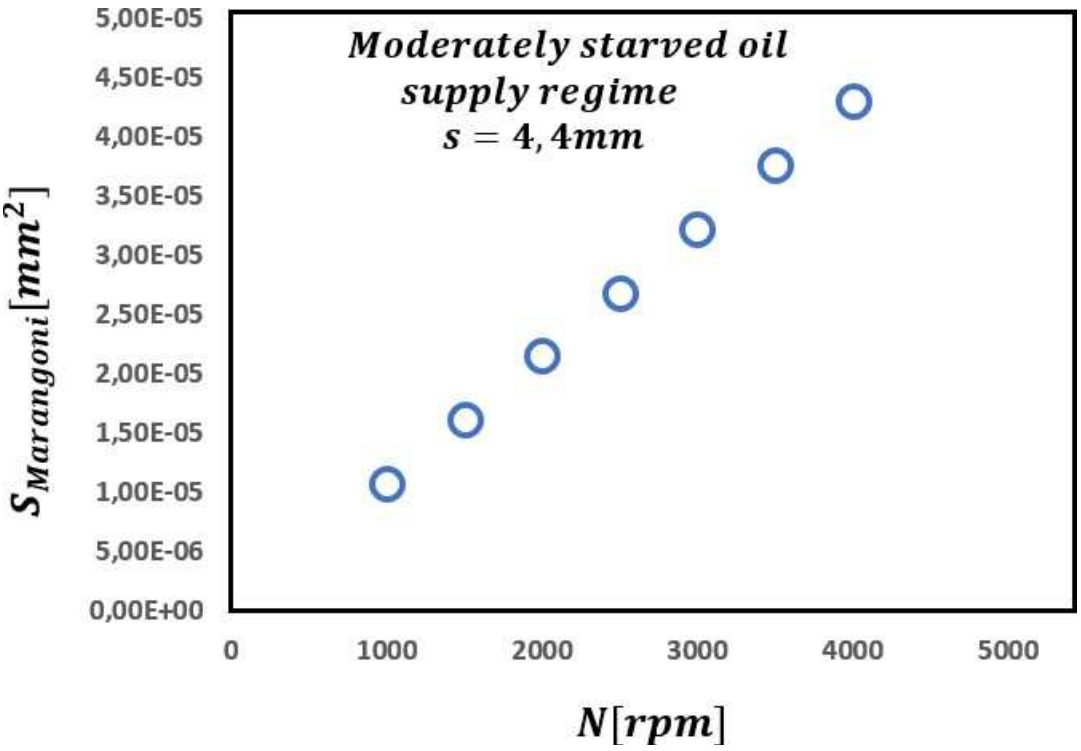

Figure 12: The surface moved due to the Marangoni effect as a function of the engine speed (N)

3.2 Lubricant redistribution

In order to study the influence of the ring passage on the oil distribution, a lubricant geometry distribution is imposed at the inlet of the contact. Figure 13 is an example of an oil distribution where the contact occurs between the liner and a parabolic ring centered at zero. The oil geometry distribution imposed at the inlet of the contact is shown in figure 17 as the continuous-blue curve.

Using a mass-conserving solver, the pressure and oil distributions after the ring passage are obtained, see Biboulet et al. [35]. The pressure distribution obtained after the first passage of the ring is shown in figure 14. It is divided into two zones: the pressurized and the non-pressurized zones.

the pressurized zones are obtained where the oil quantity available is sufficient to generate pressure (the white zones on figure 15),

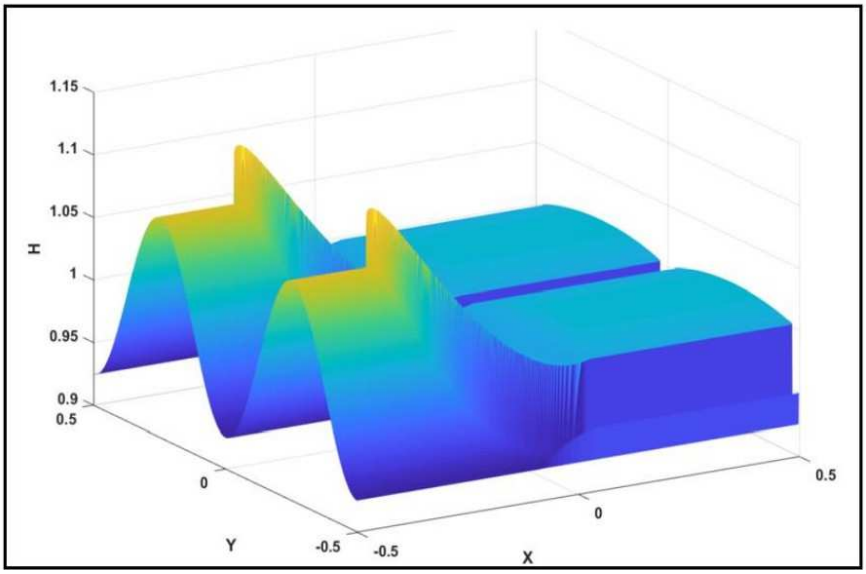

Figure 13: Lubricant geometry distribution before the ring passage along the liner

the non-pressurized zones are obtained where the pressure can not be generated as the lack of lubricant is important. They are called the cavitated zones (the grey zones on figure 15).

As shown in figure 16, presenting the pressure distribution after ten passages of the ring along the liner, the pressurized zones are almost touching. This result indicates that the ring passage along the liner redistributes the lubricant and helps to avoid starvation. The ring passage is beneficial for the lubricant distribution hence for the contact performance.

Lubricant redistribution prediction

Figure 17 presents the imposed lubricant geometry (see equation 18) before the ring passage (continuous-blue curve) and the one obtained after the ring passage (dotdash-purple curve). The lubricant redistributed as a result of the ring passage is quantified as the surface difference between the two curves ($S_{redistributed}=\Delta S_1+\Delta S_2$). The parameters of the imposed geometry in this example are:

$H_{mean}=1$,

$H_{var}=0.075$,

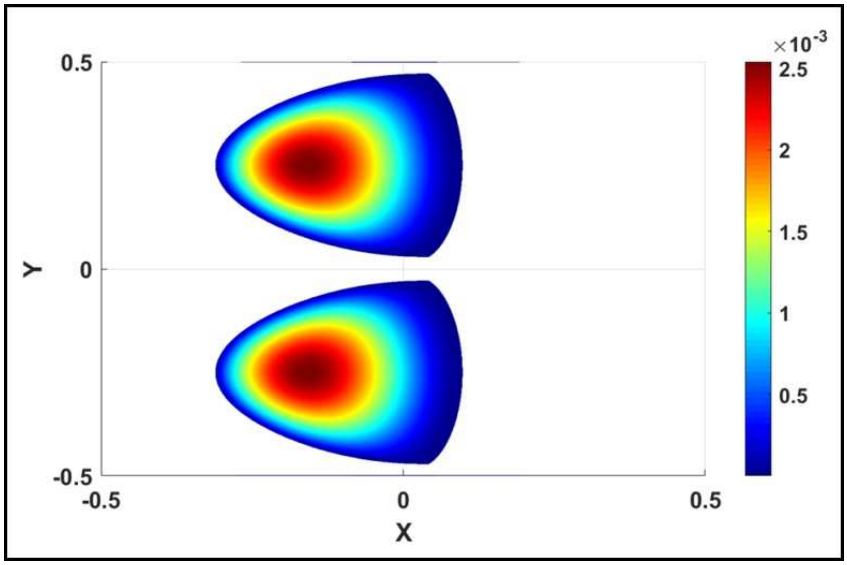

Figure 14: Pressure distribution in the contact after one passage of the ring along the liner

$\Lambda = 0.5.$

The oil redistribution ($S_{redistributed}$) caused by the ring passage along the liner is studied as a function of the minimum oil film thickness (h_0), the wavelength of the initial oil geometry distribution (λ) and the number of passages (*passage*).
The numerical results have then been fitted in order to predict the redistribution as a function of the problem parameters.
The obtained curve fit equation is:

$$S_{redistributed} = \xi\,(h_{mean} - h_0 + h_{var})^{1.125} \quad \left(\frac{\lambda}{passage^2}\right)^{0.875} \tag{23}$$

where ξ is the curve fit parameter which is a constant.

Influence of the oil film thickness: Figure 18 shows that the redistribution increases with the oil film thickness. The redistribution depends on the oil quantity supplied to the contact, it is more important when the oil supply is more pronounced. In fact, the redistribution is a result of the pressure gradient generated by the lubricant.

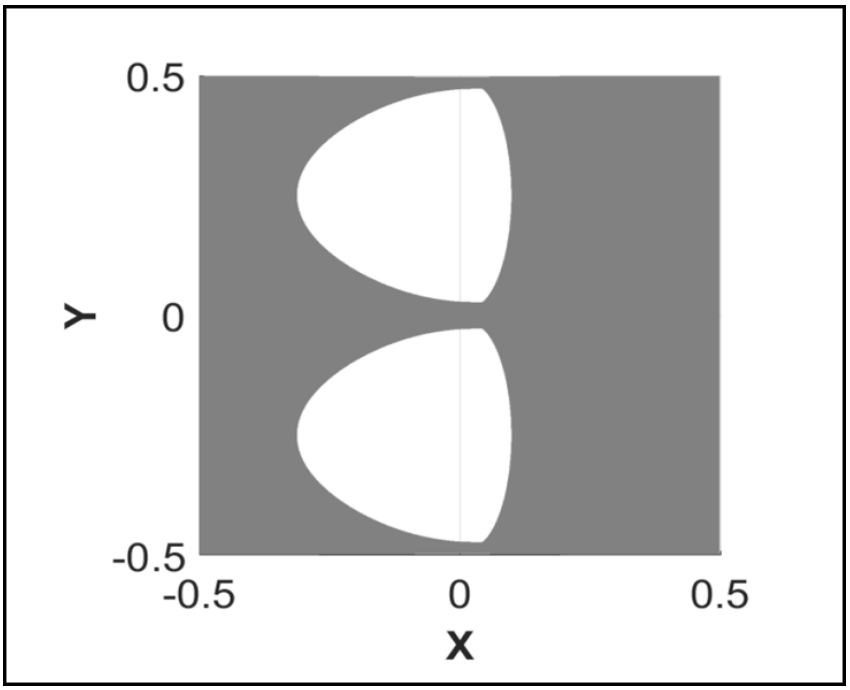

Figure 15: Cavitated zones after one passage of the ring along the liner

Influence of the wavelength: The wavelength of the oil distribution geometry impacts the lubricant redistribution. When the wavelength decreases, the number of cavitated zones increases. In this study, the redistribution occurring at each cavitated zone is quantified separately. Results show that the redistribution increases with the wavelength (figure 19).

Influence of the number of passages: The redistribution is a repetitive process that takes place at each passage of the ring along the liner. Figure 20 shows that the redistribution slows down with the number of passages or with time since the oil quantity available in the non cavitated zones decreases after each passage. Note that as the lubricant distribution occurring between two passages is the main interest of this study, the number of passages is limited to 1.

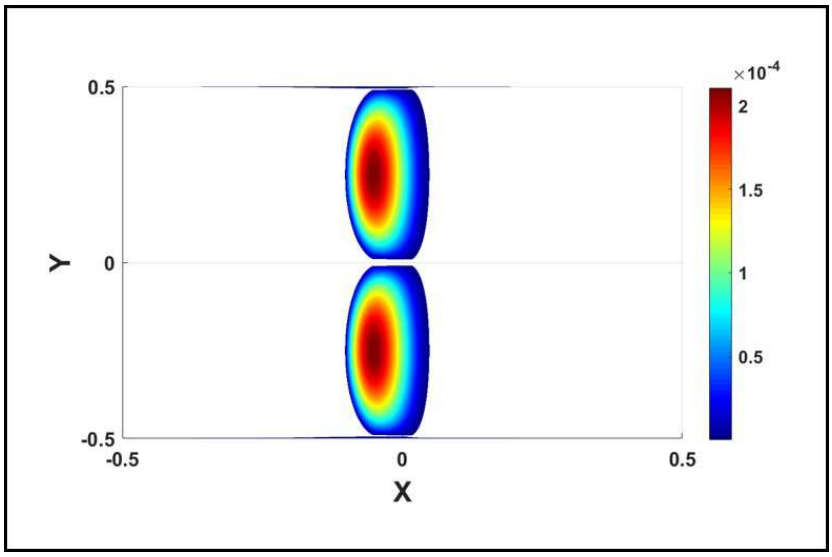

Figure 16: Pressure distribution in the contact after ten passages of the ring along the liner

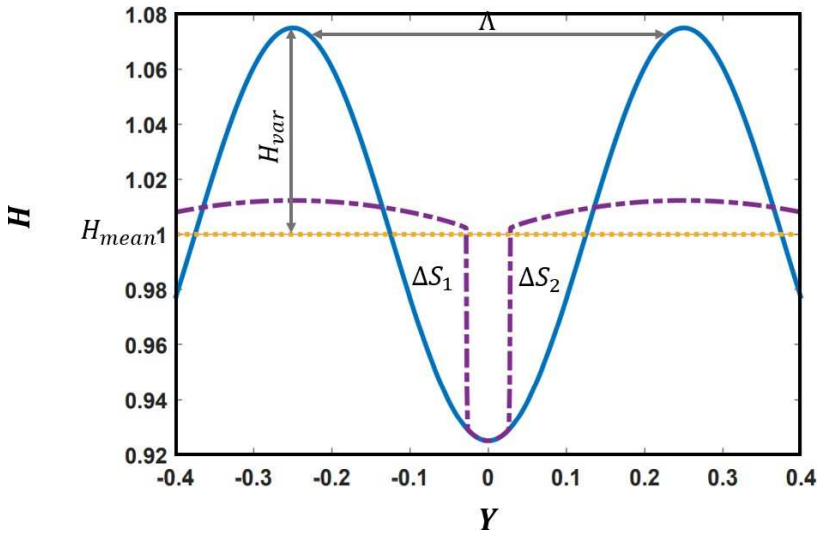

Figure 17: Lubricant distribution before and after the ring passage

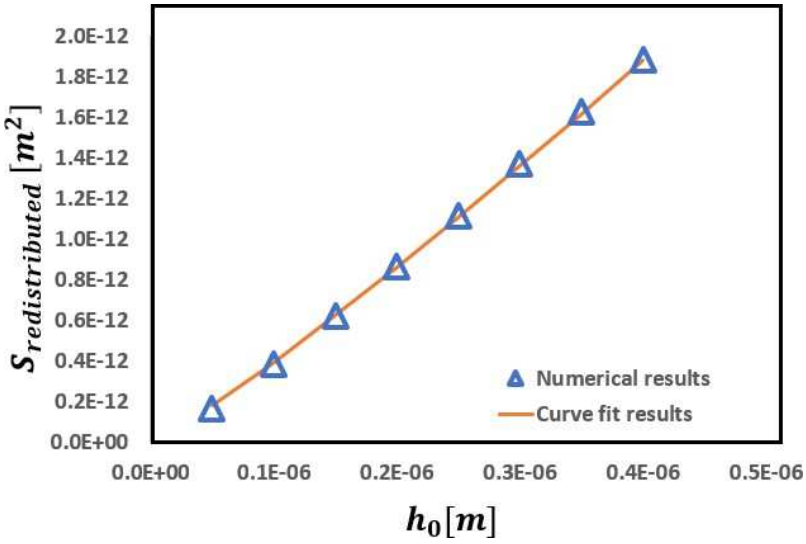

Figure 18: Numerical results and curve-fit of the surface redistributed as a function of h_0

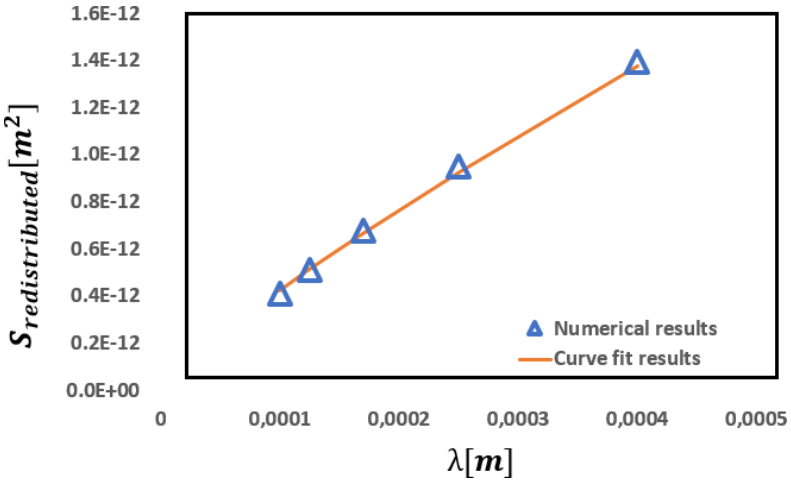

Figure 19: Numerical results and curve-fit of the surface redistributed as a function of λ

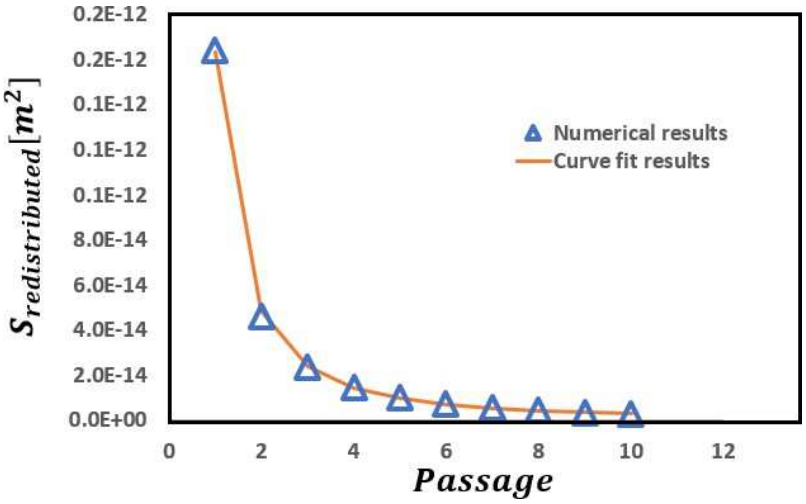

Figure 20: Numerical results and curve-fit of the surface redistributed as a function of the number of passages

3.3 Scuffing initiation limit

The algorithm presented in paragraph 2.4 quantifies the oil displaced due to the Marangoni effect ($S_{Marangoni}$) and the oil redistributed due to the ring displacement effect ($S_{redistributed}$) as a function of the operating parameters. Then, the surfaces moved are compared in order to study the scuffing initiation limit. When the two surfaces are balanced, further lack of lubricant is prevented, hence, starvation is limited and scuffing is avoided. Therefore, the contact performs normally, this is called the safe zone. Whilst, when the Marangoni effect predominates the ring passage effect, starvation is not limited and scuffing might initiate. In this case, the contact no longer operates in the safe zone.

The scuffing initiation limit is presented as a curve. The safe zone where scuffing is prevented is located below this curve. Whilst above it, scuffing can occur. The limit is studied as a function of the model parameters such as the contact load (ring tension), the engine speed (N) and the thermal parameters as the heated zone width (s) and the local temperature increase (ΔT). This section intends to present the dependency of the scuffing initiation limit as a function of these parameters.

3.3.1 Influence of the thermal parameters

Figure 21 is a chart giving the scuffing initiation limit as a function of the ring tension and the local temperature increase for different widths of the heated zone and a moderately starved oil supply regime.

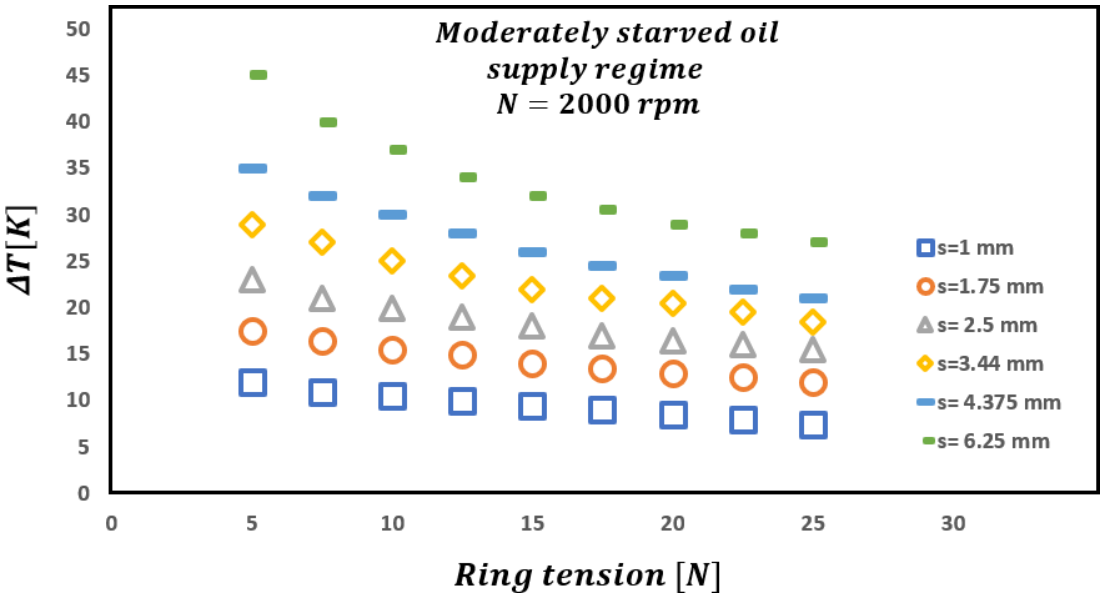

Figure 21: Scuffing initiation limit as a function of ring tension (F_{ring}) and surface temperature increase (ΔT)

From this chart, two vital conclusions can be drawn:

for the same ring tension and surface temperature increase, the scuffing initiation limit shifts up by increasing the width of the heated zone. Thus, the safe zone becomes wider,

for the same width of the heated zone and by increasing the ring tension, scuffing might be reached sooner. In fact, the ring tension has an influence on the oil film thickness (the higher the ring tension, the lower the oil film thickness). The latter in turn affects the moved surfaces as shown in equations 20 and 23.

The temperature increase is a vital variable impacting the oil displacement caused by the Marangoni effect. The higher the temperature increase, the larger the surface

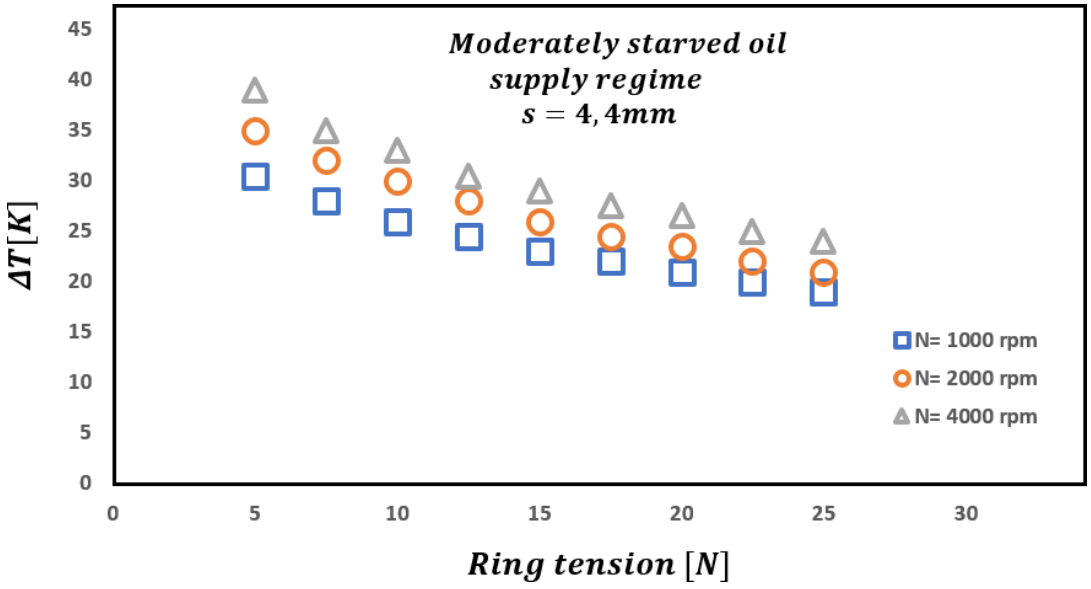

Figure 22: Scuffing initiation limit as a function of ring tension and surface temperature increase for different engine speeds

moved due to the Marangoni effect. Based on this conclusion, the influence of the Marangoni effect is more important when the temperature gradient increases.

3.3.2 Influence of the engine speed

Figure 22 presents the scuffing initiation limit for different engine speeds. It shows that the scuffing initiation limit is shifted up when the engine speed increases. In fact, the surface displaced due to the Marangoni effect increases with the engine speed due to the increase in the oil film thickness as shown previously in figure 12. Moreover, the surface redistributed due to the ring displacement effect increases also with the oil film thickness which increases with the engine speed as shown in figure 18. The balance between the moving surfaces seems to be more pronounced when the engine speed increases thus scuffing initiation is delayed.

4 Conclusion

This paper presents the influence of two opposing effects on the lubricant distribution and their complementary contribution to scuffing initiation risk in a PRCL contact. The first one is the Marangoni effect, which tends to create a local lack of lubricant due to the temperature gradient generated on the surface. The lubricant tends to flow from the high-temperature zones to the low-temperature zones because of the lubricant surface tension gradient. This lubrication condition might be one of the causes that accelerates scuffing initiation. The second effect is the ring passage along the liner. It redistributes the oil in the contact. This redistribution helps to avoid local starvation and might have an important role in delaying scuffing initiation. This work shows that when the contact is exposed to heating, its lubrication conditions are affected and temporarily starvation can occur. After re-lubricating the contact, two cases can occur. If starvation is balanced with the re-lubrication, the heating is avoided and the contact operates in the safe zone, it performs normally. Else, if starvation is not balanced by the re-lubrication, meaning that the heating is not avoided, the contact no longer operates in the safe zone and a risk of scuffing initiation exists. A computational model was developed and charts were generated illustrating the scuffing limit as curves as a function of the problem parameters. These charts provide new insights for scuffing initiation prediction in the PRCL contact of engines.

5 Appendix

5.1 Discretization and resolution

The equations are solved numerically using MATLAB software.

5.1.1 Thermal Fourier equation

The thermal system to be solved (see figure 4) for the Marangoni calculation is:

$$[A]\{\bar{T}\} = \{f\} \tag{24}$$

where A is a matrix, $\bar{T}$ is the unknown temperature field vector to be calculated and f is the right hand side depending on the boundaries conditions. The heat equation and the Neumann boundary condition (surface flux) are discretized using a second order centered scheme as shown in the equation below:

$$\frac{\bar{T}_{j+1,k} - 2\bar{T}_{j,k} + \bar{T}_{j-1,k}}{(\Delta Y)^2} + \frac{\bar{T}_{j,k+1} - 2\bar{T}_{j,k} + \bar{T}_{j,k-1}}{(\Delta Z)^2} = 0 \tag{25}$$

where j and k are Y and Z indices respectively, ΔY and ΔZ are the space mesh sizes. The equation below gives the discretization of the boundary condition:

$$Q_{j,k} = \frac{\bar{T}_{j,k+1} - \bar{T}_{j,k-1}}{2\Delta Z} \tag{26}$$

As the flux boundary condition is imposed on the surface (k=0), the ghost points method is applied to the discretization, where the points at k=-1 are virtual.

$$Q_{j,0} = \frac{\bar{T}_{j,1} - \bar{T}_{j,-1}}{2\Delta Z} \tag{27}$$

Once the system is defined, the temperature field is calculated by a simple matrix calculation:

$$\{\bar{T}\} = [A]^{-1}\{f\} \tag{28}$$

5.1.2 Marangoni equation

The Marangoni equation is a 1D parabolic equation. The discretization of the equation in space and time is given by the equation below:

$$H_j^{n+1} = H_j^n - \frac{\Delta \bar{t}}{\Delta Y^2} \frac{\bar{\gamma}_{j+1} - \bar{\gamma}_j}{4} \frac{(H_{j+1} + H_j)^2}{(\bar{\eta}_{j+1} + \bar{\eta}_j)} - \frac{\Delta t}{\Delta Y^2} \frac{\bar{\gamma}_{j-1} - \bar{\gamma}_j}{4} \frac{(H_{j-1} + H_j)^2}{(\bar{\eta}_{j-1} + \bar{\eta}_j)} \tag{29}$$

where n and j are time and space indices respectively, ΔY is the space mesh size and $\Delta \bar{t}$ is the time step.

5.2 Dimensionless variables

The thermal and hydrodynamic dimensionless variables are detailed respectively in table 1 and table 2.

x_0	y_0	z_0	T_0	γ_0	η_0	t_0	q_0
s	s	s	T_0	γ_{T_0}	η_{T_0}	$s^2\eta_0/h_0\gamma_0$	$\alpha T_0/s$

Table 1: Thermal dimensionless parameters

x_0	y_0	λ_0	h_0	p_0
a	a	a	h_0	$12\eta u_m a/h_0^2$

Table 2: Hydrodynamic dimensionless parameters

5.3 Numerical model input parameters

Table 3 and table 4 give respectively the chosen geometric and operating parameters. The values of the ring geometry parameters are typical ones. Likewise for the operating parameters. Concerning the heated zone width, its value is small enough to model a localized heated zone and wide enough to cause a temperature gradient that perturbs the operating conditions of the contact.

Variable	Symbol	Unit	Value
Nominal ring diameter	φ	mm	75.4
Axial ring thickness	t_{axial}	mm	1.5
Ring radius of curvature	R_x	mm	10
Heated zone width	s	mm	[1; 6.25]
Calculationnal domain width	s_d	mm	50
Calculationnal domain thickness	e_d	mm	2.5
Surface roughness	σ	μm	0.2

Table 3: Geometric parameters

Variable	Symbol	Unit	Value
Stroke length	C	cm	10
Engine speed	N	rpm	[1000; 4000]
Initial surface tension	γ_0	N/m	0.38
Initial viscosity	η_0	$Pa.s$	0.0081
Initial temperature	T_0	K	363
Ring tension	$F_{tension}$	N	[5; 25]

Table 4: Operating parameters

Notation

α material conductivity [$W/m/K$]

$\bar{\eta}$ dimensionless viscosity ($\bar{\eta} = \eta/\eta_0$) [$-$]

$\bar{\gamma}$ dimensionless surface tension ($\bar{\gamma} = \gamma/\gamma_0$) [$-$]

$\bar{T}$ dimensionless temperature ($\bar{T} = T/T_0$)

$\bar{t}$ dimensionless time ($\bar{t} = t/t_0$)

ΔT temperature increase [K]

η viscosity [$Pa.s$]

γ surface tension [N/m]

Λ dimensionless wavelength ($\Lambda = \lambda/lambda_0$)

λ film wavelength [m]

μ coefficient of friction

σ surface roughness [m]

ϑ void fraction

a hydrodynamic domain width [m]

C stroke length [m]

e_d thermal domain thickness [m]

f engine frequency [Hz]

F_{ring} ring tension [N]

$F_{tension}$ ring tension [N]

H Dimensionless film thickness

h_0 oil film thickness [m]

H_{mean} dimensionless mean film thickness ($H_{mean} = h_{mean}/h_0$)

h_{mean} mean film thickness [m]

H_{var} dimensionless film variation ($H_{var} = h_{var}/h_0$)

h_{var} film variation with respect to h_{mean} [m]

N engine frequency [rpm]

P dimensionless pressure

p pressure [Pa]

$p_{contact}$ contact pressure [Pa]

phi nominal ring diameter temperature [m]

phi_c Couette flux [m^2/s]

Q dimensionless heat flux ($Q = q/q_0$)

$q_{heated-zone}$ heat flux in the starved zone [W/m^2]

q_{mean} averaged heat flux [W/m^2]

R_x ring radius of curvature [m]

s width of the heated zone [m]

s_d thermal domain size [m]

T temperature [K]

T temperature [K]

t time [s]

T_0 reference temperature [K]

t_{axial} axial ring thickness [m]

$tau_{Marangoni}$ Marangoni stress [N/m^2]

$tau_{viscous}$ viscous stress [N/m^2]

u_m mean ring velocity [m/s]

v lubricant velocity [m/s]

w_1 contact load per unit length [N/m]

X dimensionless axial coordinate ($X = x/x_0$)

x axial direction coordinate

Y dimensionless circumferential coordinate ($Y = y/y_0$)

y circumferential direction coordinate

Z dimensionless depth coordinate ($Z = z/z_0$)

z depth direction coordinate

6 Acknowledgments

The Armand Peugeot Chair in cooperation with Stellantis (Fusion between Groupe PSA and FCA Group), National Institute of Applied Sciences of Lyon (INSA-Lyon), LaMCoS laboratory, fund Dahdah's thesis under the 'ANRT-CIFRE' contract n 2018/0816.

References

[1] S. C. Tung and M. L. McMillan, “Automotive tribology overview of current advances and challenges for the future,” Tribology International, vol. 37, no. 7, pp. 517–536, 2004.

[2] K. C. Ludema, “A review of scuffing and running-in of lubricated surfaces, with asperities and oxides in perspective,” Wear, vol. 100, no. 1-3, pp. 315–331, 1984.

[3] F. Saeidi, S. Shevchik, and K. Wasmer, “Automatic detection of scuffing using acoustic emission,” Tribology International, vol. 94, pp. 112–117, 2016.

[4] M. Tas, A. Banerji, M. Lou, M. Lukitsch, and A. Alpas, “Roles of mirror-like surface finish and dlc coated piston rings on increasing scuffing resistance of cast iron cylinder liners,” Wear, vol. 376, pp. 1558–1569, 2017.

[5] A. Dyson, “The failure of elastohydrodynamic lubrication of circumferentially ground discs,” Proceedings of the Institution of Mechanical Engineers, vol. 190, no. 1, pp. 699–711, 1976.

[6] A. de Gee and G. Rowe, “Glossary of terms and definitions in the field of friction, wear and lubrication tribology,” Organization for Economic Co-operation and Development, Paris, 1969.

[7] A. ASTM, “Standard terminology relating to wear and erosion,” G40, 2013.

[8] M. Shuster, D. Combs, K. Karrip, and D. Burke, “Piston ring cylinder liner scuffing phenomenon studies using acoustic emission technique,” SAE transactions, pp. 901–913, 2000.

[9] P. Obert, T. Müller, H.-J. Füßer, and D. Bartel, “The influence of oil supply and cylinder liner temperature on friction, wear and scuffing behavior of piston ring cylinder liner contacts–a new model test,” Tribology International, vol. 94, pp. 306–314, 2016.

[10] M. Shen, H. Cheng, and P. Stair, “Scuffing failure in heavily loaded slow speed conformal sliding contacts,” 1991.

[11] B. Li, C. H. Wong, and Q. Chen, “Kinetics of lubricant desorption and decomposition under heat treatment: a molecular dynamics study,” Soft Matter, vol. 9, no. 3, pp. 700–708, 2013.

[12] J. Qu, J. J. Truhan, P. J. Blau, and H. M. Meyer III, "Scuffing transition diagrams for heavy duty diesel fuel injector materials in ultra low-sulfur fuel-lubricated environment," Wear, vol. 259, no. 7-12, pp. 1031–1040, 2005.

[13] W. Van Dam, M. W. Cooper, K. Oxorn, and S. Richards, "Observations from cylinder liner wear studies in heavy duty diesel engines and the evolution towards lower viscosity heavy duty engine lubricants," tech. rep., SAE Technical Paper, 2011.

[14] R. Barunovic, V. Haas, C. Langlade, and C. E. Krill III, "Sliding wear of 100cr6 in a diesel-lubricated flat–flat contact under realistic loads," Tribology international, vol. 53, pp. 1–11, 2012.

[15] O. Ajayi, C. Lorenzo-Martin, R. Erck, and G. Fenske, "Analytical predictive modeling of scuffing initiation in metallic materials in sliding contact," Wear, vol. 301, no. 1-2, pp. 57–61, 2013.

[16] H. Yu and J. Medley, "Influence of lubricant additives on friction in a disc machine," in Tribology Series, vol. 32, pp. 475–486, Elsevier, 1997.

[17] S. Wan, D. Li, A. K. Tieu, B. Zhang, et al., "Comparison of the scuffing behaviour and wear resistance of candidate engineered coatings for automotive piston rings," Tribology International, vol. 106, pp. 10–22, 2017.

[18] M. Kennedy, S. Hoppe, and J. Esser, "Lower friction losses with new piston ring coating," MTZ worldwide, vol. 75, no. 4, pp. 24–29, 2014.

[19] I. Etsion, G. Halperin, and E. Becker, "The effect of various surface treatments on piston pin scuffing resistance," Wear, vol. 261, no. 7-8, pp. 785–791, 2006.

[20] A. Riahi, T. Perry, and A. Alpas, "Scuffing resistances of al–si alloys: effects of etching condition, surface roughness and particle morphology," Materials Science and Engineering: A, vol. 343, no. 1-2, pp. 76–81, 2003.

[21] Z. Ye, C. Zhang, Y. Wang, H. Cheng, S. Tung, Q. J. Wang, and X. He, "An experimental investigation of piston skirt scuffing: a piston scuffing apparatus, experiments, and scuffing mechanism analyses," Wear, vol. 257, no. 1-2, pp. 8–31, 2004.

[22] Y. Wang, C. Yao, G. Barber, B. Zhou, and Q. Zou, "Scuffing resistance of coated piston skirts run against cylinder bores," Wear, vol. 259, no. 7-12, pp. 1041–1047, 2005.

[23] Y. Wang, K. Brogan, and S. C. Tung, “Wear and scuffing characteristics of composite polymer and nickel/ceramic composite coated piston skirts against aluminum and cast iron cylinder bores,” Wear, vol. 250, no. 1-12, pp. 706–717, 2001.

[24] S. Bewsher, M. Mohammadpour, H. Rahnejat, G. Offner, and O. Knaus, “An investigation into the oil transport and starvation of piston ring pack,” Proceedings of the Institution of Mechanical Engineers, Part J: Journal of Engineering Tribology, vol. 233, no. 1, pp. 112–124, 2019.

[25] I. Sherrington, “Measurement techniques for piston-ring tribology,” Tribology and Dynamics of Engine and Powertrain, pp. 387–425, 2010.

[26] M. Gore, M. Theaker, S. Howell-Smith, H. Rahnejat, and P. D. King, “Direct measurement of piston friction of internal-combustion engines using the floating-liner principle,” Proceedings of the Institution of Mechanical Engineers, Part D: Journal of Automobile Engineering, vol. 228, no. 3, pp. 344–354, 2014.

[27] P. Mishra, S. Balakrishnan, and H. Rahnejat, “Tribology of compression ring- to-cylinder contact at reversal,” Proceedings of the Institution of Mechanical Engineers, Part J: Journal of Engineering Tribology, vol. 222, no. 7, pp. 815–826, 2008.

[28] P. Mishra, H. Rahnejat, and P. King, “Tribology of the ring bore conjunction subject to a mixed regime of lubrication,” Proceedings of the Institution of Mechanical Engineers, Part C: Journal of Mechanical Engineering Science, vol. 223, no. 4, pp. 987–998, 2009.

[29] X. Fanton and A. Cazabat, “Spreading and instabilities induced by a solutal marangoni effect,” Langmuir, vol. 14, no. 9, pp. 2554–2561, 1998.

[30] R. Monti, R. Savino, and S. Tempesta, “Wetting prevention by thermal marangoni effect. experimental and numerical simulation,” European Journal of Mechanics-B/Fluids, vol. 17, no. 1, pp. 51–77, 1998.

[31] M. Gugliotti, M. S. Baptista, and M. J. Politi, “Surface tension gradients induced by temperature: The thermal marangoni effect,” Journal of chemical education, vol. 81, no. 6, p. 824, 2004.

[32] M. Organisciak, G. Cavallaro, and A. Lubrecht, “Variable lubricant supply of a starved hydrodynamic linear contact: lubricant lateral flow for smooth and

laser textured surfaces," Proceedings of the Institution of Mechanical Engineers, Part J: Journal of Engineering Tribology, vol. 221, no. 3, pp. 247–258, 2007.

[33] Y. Hu, X. Meng, and Y. Xie, "A new efficient flow continuity lubrication model for the piston ring-pack with consideration of oil storage of the cross-hatched texture," Tribology International, vol. 119, pp. 443–463, 2018.

[34] R. Rahmani, H. Rahnejat, B. Fitzsimons, and D. Dowson, "The effect of cylinder liner operating temperature on frictional loss and engine emissions in piston ring conjunction," Applied energy, vol. 191, pp. 568–581, 2017.

[35] N. Biboulet and A. Lubrecht, "Efficient solver implementation for reynolds equation with mass-conserving cavitation," Tribology International, vol. 118, pp. 295–300, 2018.

[36] H. Moes, "Lubrication and beyond," University of Twente lecture notes, vol. 115531, p. 366, 2000.